SCIENTIFIC REPORTS

OPEN

Tuneable Magnetic Phase Transitions in Layered $CeMn_2Ge_{2-x}Si_x$ Compounds

Received: 01 September 2014
Accepted: 12 May 2015
Published: 19 June 2015

M. F. Md Din[1,4], J. L. Wang[1,2], Z. X. Cheng[1], S. X. Dou[1], S. J. Kennedy[2], M. Avdeev[2] & S. J. Campbell[3]

The structural and magnetic properties of seven $CeMn_2Ge_{2-x}Si_x$ compounds with x = 0.0–2.0 have been investigated in detail. Substitution of Ge with Si leads to a monotonic decrease of both a and c along with concomitant contraction of the unit cell volume and significant modifications of the magnetic states - a crossover from ferromagnetism at room temperature for Ge-rich compounds to antiferromagnetism for Si-rich compounds. The magnetic phase diagram has been constructed over the full range of $CeMn_2Ge_{2-x}Si_x$ compositions and co-existence of ferromagnetism and antiferromagnetism has been observed in $CeMn_2Ge_{1.2}Si_{0.8}$, $CeMn_2Ge_{1.0}Si_{1.0}$ and $CeMn_2Ge_{0.8}Si_{1.2}$ with novel insight provided by high resolution neutron and X-ray synchrotron radiation studies. $CeMn_2Ge_{2-x}Si_x$ compounds (x = 0, 0.4 and 0.8) exhibit moderate isothermal magnetic entropy accompanied with a second-order phase transition around room temperature. Analysis of critical behaviour in the vicinity of T_C^{inter} for $CeMn_2Ge_2$ compound indicates behaviour consistent with three-dimensional Heisenberg model predictions.

Due to the wide and interesting range of structural and magnetic phenomena - including magnetism, superconductivity, mixed valence, Kondo behaviour and heavy fermion - exhibited by layered RT_2X_2 rare earth compounds, (R is a rare earth, T is transition metal and X is Si or Ge) this series has attracted significant attention over the years (e.g.[1–4]). Most of the layered RT_2X_2 crystallize in the body centred tetragonal $ThCr_2Si_2$-type structure with space group *I4/mmm* in which the R, T and X atoms occupy the 2*a*, 4*d* and 4*e* sites respectively, with the different atoms stacked along the *c*-axis in the layered sequence R–X–T–X–R[5–7]. An important factor in the continued interest in the RMn_2X_2 over the past two decades is that the magnetic states of the Mn-sublattice depend sensitively on the inter-planar and intra-planar Mn–Mn distances[8,9]. Furthermore, intensive studies of RMn_2X_2 compounds have revealed a large variety of magnetic structures and magnetic phase transitions that occur with changes in chemical composition, temperature and mechanical pressure or magnetic field applied[10–12]. From this point of view, RMn_2X_2 compounds provide model systems for study of, for example, the volume dependence of magnetic ordering. They also offer scope for design of critical magnetic parameters — such as the type or order of magnetic phase transitions and ability to shift transition temperatures — by controlling the intra-planar separation distance $d^a_{Mn\text{-}Mn}$ with applied mechanical or chemical pressure via replacement with elements of different atomic sizes[13–15].

In this study, we report the findings of an investigation of the effects of substituting Si for Ge in $CeMn_2Ge_{2-x}Si_x$ (x = 0.0–2.0) on their magnetic properties and structures using magnetic, differential

[1]Institute for Superconductivity and Electronic Materials, University of Wollongong, Wollongong, NSW 2522, Australia. [2]Bragg Institute, Australian Nuclear Science and Technology Organization, Lucas Heights, NSW 2234, Australia. [3]School of Physical, Environmental and Mathematical Sciences, The University of New South Wales, Canberra, ACT 2600, Australia. [4]Department of Electrical & Electronic Engineering, Faculty of Engineering, National Defence University of Malaysia, Kem Sungai Besi, 57000 Kuala Lumpur, Malaysia. Correspondence and requests for materials should be addressed to M.F.M.D. (email: mfmd999@uowmail.edu.au) or J.L.W. (email: jianli@uow.edu.au)

scanning calorimetry (DSC), high resolution X-ray synchrotron radiation and neutron diffraction measurements. In addition to exploring the effects of the Si atoms on the metalloid Ge, it is expected that substitution of Ge (atomic radius 1.37 Å) with the smaller Si (atomic radius 1.32 Å) would modify the magnetic structures of $CeMn_2Ge_{2-x}Si_x$. This follows as $d^a_{Mn\text{-}Mn} \sim 2.93$ Å in $CeMn_2Ge_2$ while $d^a_{Mn\text{-}Mn} \sim 2.83$ Å in $CeMn_2Si_2$[16] ($d^a_{Mn\text{-}Mn}$ is the Mn–Mn separation distance in the *ab*-plane). These values of $d^a_{Mn\text{-}Mn}$ are respectively greater than $d_{crit1} \sim 2.87$ Å (of related lattice parameter $a_{crit1} = 4.06$ Å) and less than $d_{crit2} \sim 2.84$ Å (related lattice parameter $a_{crit2} = 4.02$ Å), the first and second critical intralayer Mn–Mn distances which govern the magnetic behaviour in RMn_2X_2 compounds[17,18]. According to Welter *et al.*[19], the $d^a_{Mn\text{-}Mn}$ not only affects the intralayer Mn–Mn coupling but also the interlayer exchange interaction and, as summarised below, three general categories can be delineated[20].

(i) $d^a_{Mn\text{-}Mn} > d_{crit1} = 2.87$ Å: The interlayer exchange coupling is ferromagnetic and the intralayer coupling antiferromagnetic; this leads to the canted Fmc-type ferromagnetic structure (see detailed definition of magnetic structures in Figure S1 of the Supplementary Material; the Fmc structure can be described by the Im-m2- magnetic space group (Opechowski-Guccione #44.3.326, basis (b,c,a;0 0 0); active vector (0,0,0)).

(ii) $d_{crit2} = 2.84$ Å $< d^a_{Mn\text{-}Mn} < d_{crit1} = 2.87$ Å; Both the interlayer and the intralayer coupling are antiferromagnetic; this leads to the AFmc-type magnetic structure. AFmc structure can be described by the Pnnm' magnetic space group (Opechowski-Guccione #58.4.474, basis (-a, c, b; 0,0,0); active vector (0,0,1)).

(iii) $d^a_{Mn\text{-}Mn} < d_{crit2} = 2.84$ Å; No intralayer in-plane spin component and antiferromagnetic interlayer coupling; this leads to the AFil-type magnetic structure which can be described by $I_P4/m'm'm'$ magnetic space group (Opechowski-Guccione #139.17.1195; basis (a, b, c; 1/4, 1/4, 1/4); active vector (0,0,1)).

The interest in the properties and behaviour of layered structure materials has been enhanced in recent years by the discovery of a giant magnetocaloric effect (MCE) near room temperature in $Gd_5Si_2Ge_2$ compound[21–23]. $R_5(Si,Ge)_4$ type compounds have a distinct layered structure in which the covalent Si–Si, Si–Ge and Ge–Ge bonds and interlayer distances play a vital role in determining their magnetic and magnetocaloric effect properties[22]. This in turn has led to an increased focus on understanding the fundamental properties of this type of layered material. As already noted, the $CeMn_2Ge_{2-x}Si_x$ system has a sequence of atomic layers stacked along the *c*-axis similar to the $R_5(Si,Ge)_4$ system. Also as noted, the relatively simple body centred tetragonal $ThCr_2Si_2$-type structure offers scope for selection of the magnetic state via the strong dependence of Mn–Mn intraplanar and interplanar exchange interactions on $d^a_{Mn\text{-}Mn}$ the Mn–Mn separation distance in the *ab*-plane. This information is expected to provide enhanced understanding of the correlation between magnetic properties and atomic distances. Our comprehensive investigation of the crystallographic, magnetic properties and critical exponent behaviour of $CeMn_2Ge_{2-x}Si_x$ compounds ($x = 0.0$–2.0) has enabled us to establish the magnetic structures across the Ge-Si concentration range and derive the magnetic phase diagram of $CeMn_2Ge_{2-x}Si_x$.

Results

Crystal structure and magnetic phase transitions. Rietveld refinements (FULLPROF package[24]) of the room temperature X-ray diffraction patterns indicate that all of the $CeMn_2Ge_{2-x}Si_x$ samples crystallize in the $ThCr_2Si_2$ structure. The refined results — including lattice parameters *a*, *c*, axial ratio *c*/*a* and unit cell volume V — are shown in Fig. 1. As expected, substitution of Ge by Si leads to a monotonic decrease of both *a* and *c* along with concomitant contraction of the unit cell volume with increasing Si content; good agreement is obtained with published results[16]. However, it is noted that the variations of the lattice parameters and unit cell volume with composition change slope around x = 1.0–1.2 (the linear behaviour in lattice parameters expected from Vegard's Law is shown by the dotted line). The deviation from Vegard's Law is also evident in the composition dependence of the axial ratio *c*/*a* in Fig. 1.

The change in slope discerned around $x = 1.0$–1.2 is likely to be related to the change in magnetic ordering of the Mn-sublattice as in discussion of the neutron diffraction results below. At room temperature the $x = 1.2$ compound exhibits a mixture of ferromagnetic and antiferromagnetic states while compounds with $x > 1.2$ are purely antiferromagnetic. Similar tendencies in the composition dependence of the lattice constants have been detected in the related $PrMn_2Ge_{2-x}Si_x$ system[25,26]. As is well known and as indicated above (see also Fig. 1), RMn_2X_2 (X = Ge or Si) compounds exhibit different magnetic behaviours around two critical values of the lattice parameter[9]. The bond lengths between different sites have also been calculated with the BLOKJE program[27] using the structural and positional parameters and the 12-coordinate metallic radii of 1.81 Å, 1.35 Å, 1.37 Å and 1.32 Å for Ce, Mn, Ge and Si, respectively. It was found that the Mn–Mn intralayer distance at room temperature decreased from $d_{Mn\text{-}Mn} = 2.93$ Å at $x = 0$ to $d_{Mn\text{-}Mn} = 2.83$ Å at $x = 2.0$. Moreover if we assume that the contraction of the unit cell volume due to Si substitution (i.e. causing an effective chemical pressure compared with the reference $CeMn_2Ge_2$ compound) is equivalent to the influence of external pressure, the corresponding pressures can be derived to be around 43.6 kbar and 128.0 kbar for $CeMn_2GeSi$ and $CeMn_2Si_2$ respectively (details shown in Figure S2 of the Supplementary Material). The chemical pressure values were calculated from the Murnaghan equation:

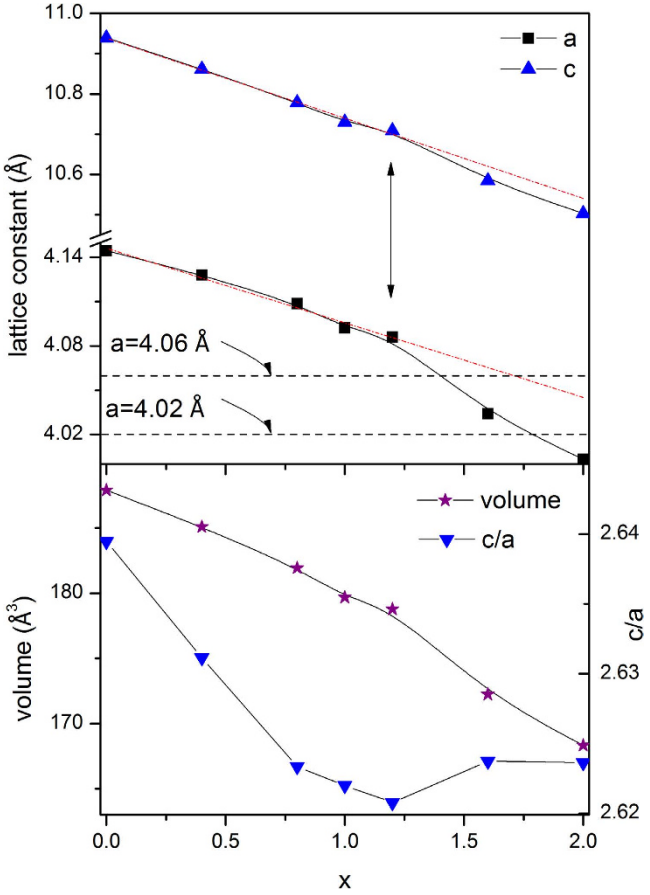

Figure 1. Composition dependence of lattice parameters *a* and *c*, axial ratio *c*/*a* and unit cell volume, V, for $CeMn_2Ge_{2-x}Si_x$ at room temperature. The arrows indicate the region where the slope changes with the dotted line denoting behaviour consistent with Vegard's law. The full lines are guides to the eye with the dashed lines of the upper figure denoting the $a_{crit1} \sim 4.06$ Å and $a_{crit2} \sim 4.02$ Å values as explained in the text.

$$p = \left(\frac{B_0}{B'_0}\right)\left[\left(\frac{V}{V_0}\right)^{-B'_0} - 1\right] \quad (1)$$

where B_0 is the isothermal bulk modulus, B'_0 its pressure derivative and V_0 and V are the volume at ambient pressure and pressure p respectively. The range of pressure values for $CeMn_2GeSi$ and $CeMn_2Si_2$ was estimated from calculations based on the modulus values $B_0 = 819$ kbar and $B'_0 = 4.0$ for $LaMn_2Si_2$[13] and $B_0 = 867$ kbar and $B'_0 = 5.1$ for $CeNi_2Ge_2$[28] (see Figure S2; it should be noted that both $LaMn_2Si_2$ and $CeNi_2Ge_2$ are isostructural with the $CeMn_2Ge_{2-x}Si_x$ compounds).

Figure 2 shows the temperature dependence of the magnetization of $CeMn_2Ge_{2-x}Si_x$ as measured in a field of 0.01 T over the temperature range of 5–340 K. Differential scanning calorimetry measurements have been used to check for possible phase transitions in the temperature region from 340 K to 550 K (details are shown in Figure S3). $CeMn_2Ge_{2-x}Si_x$ compounds reveal up to four magnetic transitions: T_N^{inter} – the Néel temperature associated with the onset of the axial component of antiferromagnetism; T_{CC} – the ferromagnetic critical temperature for incommensurate canted ferromagnetism; T_C^{inter} – the Curie temperature of the axial component of ferromagnetism and T_N^{intra}, the Néel temperature for planar antiferromagnetism. Detailed definitions of the related magnetic structures are shown in Figure S1 with details of the magnetic structures discussed below in the neutron diffraction section. Figure 2 demonstrates that below 340 K the magnetic phase transition temperatures change with the Si concentration as expected, the T_C^{inter} (magnetic phase transition temperature from interlayer antiferromagnetic AFl to canted ferromagnetic Fmc) was found to decrease from $T_C^{inter} \sim 320$ K for $x = 0.4$ to $T_C^{inter} \sim 305$ K for $x = 1.2$ (Fig. 2; inset). This behaviour may be related to the change in electronic environment as replacing Ge ($3d^{10}4s^24p^2$) by Si ($3s^23p^2$) is expected to influence the magnetic structures of the $CeMn_2Ge_{2-x}Si_x$ compounds and in addition to contracting the unit cell. This is supported by Density Functional Theory calculations for RMn_2Ge_2 (R = Y or Ca) compounds[29] which indicate that to a large extent, the magnetic

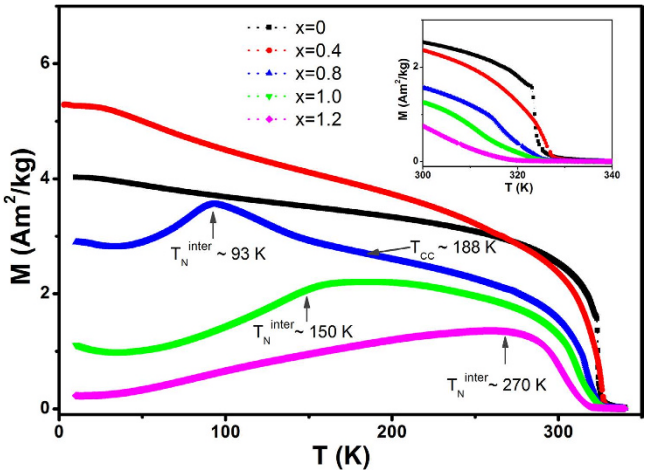

Figure 2. Temperature dependence of magnetization of $CeMn_2Ge_{2-x}Si_2$ compounds ($x = 0.0–2.0$) as measured in a field of 0.01 T. The inset shows the magnetization in the region of T_C^{inter}.

moment is determined mainly by the interatomic Mn–Mn distances, while the interstitial electron density contributes to the change in magnetic structures.

Neutron diffraction; Magnetic structures. A set of neutron powder diffraction patterns was obtained for $CeMn_2Ge_{2-x}Si_x$ compounds (x = 0.0–2.0) over the temperature range 4–450 K. Rietveld refinements were carried out on all patterns using the FULLPROF program package[24] which allows us to derive the structural and magnetic parameters. As explained fully in related articles[8,19,25,30], the specific location of Mn atoms on the 4*d* site in the $ThCr_2Si_2$ structure (space group *I4/mmm*) allows ready identification of various magnetic structures from key indicators in the neutron diffraction patterns as follows:

1. Ferromagnetic ordering of the Mn atoms—*hkl* reflections with $h + k = 2n$ and $l = 2n$ (e.g. (112), (200) reflections).
2. Antiferromagnetic ordering of the Mn atoms within the (001) planes—reflections with $h + k = 2n + 1$ (e.g. (101), (103) reflections).
3. Collinear antiferromagnetic structure between adjacent Mn planes—reflections with $h + k + l = 2n + 1$ (e.g. (111), (113) reflections).
4. Ferromagnetic mixed incommensurate structure (Fmi) of wavevector (0; 0; q_z)—satellite reflections with h + k = 2n + 1 (e.g. (101), (103)).

The neutron diffraction thermal contour plot for $CeMn_2Ge_2$ from 4–450 K shown in Fig. 3(a), covers the various magnetic regions indicated by the magnetic measurements of Fig. 2 and Figure S3. Refinement of the 450 K neutron diffraction pattern confirms that $CeMn_2Ge_2$ is paramagnetic. At 350 K (i.e. below $T_N^{intra} \sim 417$ K; Fig. 3(b)) the intensity of the (101) reflection increases and, consistent with neutron diffraction condition (2) above, $CeMn_2Ge_2$ exhibits the AFl structure. The appearance of the (112) peak at 295 K - below the transition temperature T_C^{inter} (T_{CC}) ~ 318 K - together with the presence of satellite peaks $(101)^+$, $(101)^-$ and $(103)^+$, $(103)^-$ in the patterns and noting condition (4) above, demonstrates that $CeMn_2Ge_2$ has the ferromagnetic mixed incommensurate (Fmi) magnetic structure below this transition temperature. The Fmi magnetic structure is found to persist with decrease in temperature to T ~ 4 K as confirmed by the absence of change in the intensities of the $(101)^+$ and $(101)^-$ reflections. Compared with the model reported by Fernandez-Baca *et al.*[18] using the (1 0 1-q_z) vector, we found that the vector (0 0 q_z; $q_z \sim 0.31$) not only generates the $(101)^-/(101)^+$ and $(103)^-/(103)^+$ satellite peaks in their correct positions, but also results in an excellent fit of the magnetic satellites overall. Thus we conclude that our data for the Fmi magnetic structure are best described by the vector (0 0 q_z); this is the same magnetic structure reported for $LaMn_2Ge_2$ by Venturini *et al.*[31] and for RMn_2Ge_2 with R = Ce, Pr and Nd by Welter *et al.*[19].

For $CeMn_2Ge_2$ the values of the magnetic moments at 4 K (see Table 1) are derived to be $\mu_{Total} \sim 3.16\,\mu_B$, $\mu_{ab} \sim 2.53\,\mu_B$ and $\mu_c \sim 1.9\,\mu_B$ with the magnitude of the propagation vector $q_z \sim 0.317$ (Fig. 4(a)). The propagation vector is found to decrease with increasing Si concentration with $q_z \sim 0.276$ for $CeMn_2Ge_{1.6}Si_{0.4}$ at 4 K (Table 1; detailed results for $CeMn_2Ge_{1.6}Si_{0.4}$ can be found in Figure S4). This decrease in q_z on replacement of Ge with Si in $CeMn_2Ge_2$ is similar to that detected on replacement of Mn with Fe[32] and Pr with Y or Lu[9,33] in $PrMn_2Ge_2$. The temperature dependences of the structural and magnetic parameters of $CeMn_2Ge_2$ as derived from the refinements are shown in Fig. 4(a–c). Temperature dependence of the *c*/*a* ratio reveals a significant change around $T_C^{inter} \sim 318$ K (Fig. 4(c)). This phenomenon indicates that strong coupling occurs between the magnetism and the crystal lattice in the presence of a *c*-axis component of

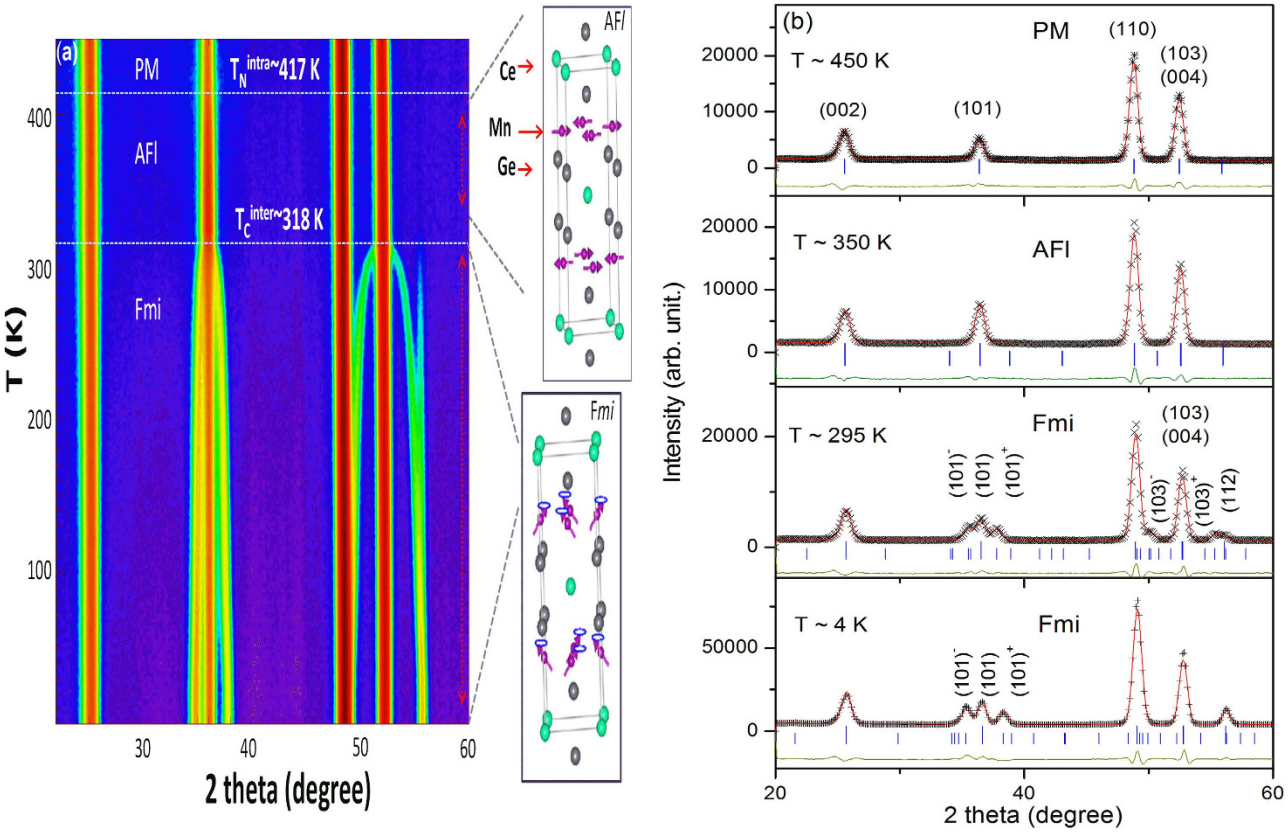

Figure 3. (**a**) Thermal contour plot of $CeMn_2Ge_2$ neutron diffraction measurements over the range of 4–450 K. The AFl and Fmi magnetic structures of $CeMn_2Ge_2$ are also shown; (**b**) Neutron diffraction patterns and Rietveld refinements for $CeMn_2Ge_2$ in different magnetic states at 450 K, 350 K, 295 K, and 4 K ($\lambda = 2.4179$ Å, Wombat diffractometer, OPAL).

Composition	$CeMn_2Ge_2$	$CeMn_2Ge_{1.6}Si_{0.4}$	$CeMn_2Ge_{0.8}Si_{1.2}$	$CeMn_2Ge_{0.4}Si_{1.6}$	$CeMn_2Si_2$
T (K)	4 K	4 K	6 K	6 K	4 K
Magnetic state	Fmi	Fmi	AFmc	AFmc	AFil
a (Å)	4.1165(4)	4.0992	4.0264	4.0049	3.9695
c (Å)	10.8723(6)	10.7942	10.6335	10.5501	10.4354
z_{Ge}	0.3821	0.3819	0.3814	0.3795	0.3816
μ_{ab} (μ_B)	2.53(3)	2.32	0.76	0.32	0
μ_c (μ_B)	1.90(5)	1.81	2.00	2.09	2.01
Canting angle	53.1	52.0	20.8	8.7	0
μ_{total} (μ_B)	3.17(7)	2.95	2.14	2.12	2.01
q_z	0.317	0.276	–	–	–
R_{wp}	5.81	7.41	9.52	5.55	7.50
R_{exp}	1.18	1.22	1.23	1.06	1.49

Table 1. Structural and magnetic parameters derived from Rietveld refinements of the neutron diffraction patterns for $CeMn_2Ge_{2-x}Si_x$ at 4 K and 6 K as indicated. The errors are shown for the $CeMn_2Ge_2$ data as an example.

the Mn moment; this behaviour is similar to that of the $PrMn_{2-x}Fe_xGe_2$ system[32], where the presence of the interlayer Mn–Mn interactions rather than the intralayer Mn–Mn interactions play the major role in the anomalous thermal expansion observed at the magnetic transition in these layered systems.

Reflecting the changes in magnetisation with temperature for the $CeMn_2Ge_{1.0}Si_{1.0}$ and $CeMn_2Ge_{0.8}Si_{1.2}$ compounds (Fig. 2), the neutron diffraction patterns of $CeMn_2Ge_{1.0}Si_{1.0}$ and $CeMn_2Ge_{0.8}Si_{1.2}$ were also

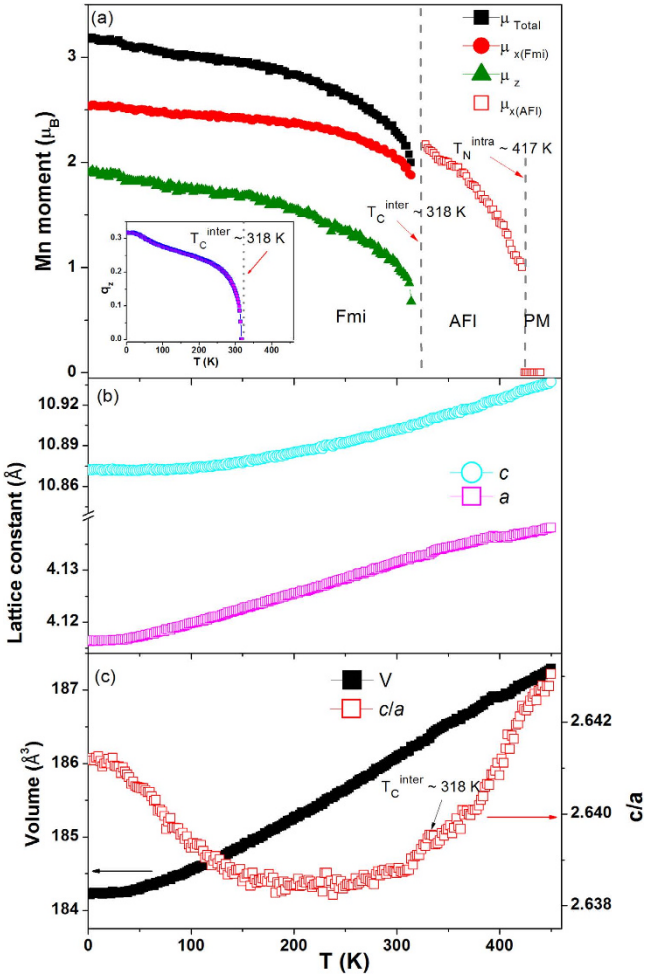

Figure 4. Structural and magnetic parameters for $CeMn_2Ge_2$ as derived from refinements of the neutron diffraction patterns of Fig. 3: (**a**) Temperature dependences of the magnetic moment and propagation vector q_z for $CeMn_2Ge_2$ (inset). T_N^{intra} and T_C^{inter} are denoted by arrows with the dotted lines delineating the paramagnetic (PM), antiferromagnetic (AFl-type) and ferromagnetic mixed incommensurate (Fmi) regions. (**b**) Temperature dependences of lattice parameters *a* and *c* and (**c**) unit cell volume and axial ratio *c*/*a*.

found to exhibit interesting behaviour. Neutron diffraction patterns were collected for both compounds over the temperature range 6–450 K with temperature steps of around 6 K in order to obtain detailed information around the phase transitions. The set of neutron diffraction patterns for $CeMn_2Ge_{0.8}Si_{1.2}$ are shown as an example in Fig. 5(a) with the refinement results at selected temperatures listed in Table 2.

Among features noted for $CeMn_2Ge_{0.8}Si_{1.2}$ are that the intensity of the (002) nuclear reflection remains effectively unchanged over the whole temperature range and the absence of satellite peak $(101)^+$, $(101)^-$ and $(103)^+$, (103) compared with $CeMn_2Ge_2$ and $CeMn_2Ge_{1.6}Si_{0.4}$. Magnetic phase transitions at $T_N^{intra} \sim 430$ K; $T_C^{inter} \sim 305$ K and $T_N^{inter} \sim 270$ K are clearly indicated by changes in the intensities of the (101), (111) and (112) reflections due to magnetic scattering, with details shown in Supplementary Figure S5. Figure S5 also indicates the temperature $T^* \sim 31$ K below which only the AFmc structure exists in $CeMn_2Ge_{0.8}Si_{1.2}$. This is evident on comparison of the diffraction patterns in Fig. 5(b) for $CeMn_2Ge_{0.8}Si_{1.2}$ at 200 K (mixed Fmc and AFmc states) with the diffraction pattern of the AFmc state at 6 K. According to neutron diffraction condition (3), the appearance of the (111) reflection peak below ~ 270 K at T ~ 200 K in Fig. 5(b) indicates the formation of the AFmc state while, based on neutron diffraction condition (2), the fact that the (112) reflection remains indicates that the Fmc state still exists at the same temperature as the mixed magnetic states behaviour. However the mixture of the Fmc and AFmc magnetic states starts to disappear when cooling to $T^* < 31$ K as the (112) reflection is absent and the (111) peak intensity remains unchanged; this behaviour indicates the occurrence of the AFmc state (see Fig. 5(b) for $CeMn_2Ge_{0.8}Si_{1.2}$ at T ~ 6 K).

Direct evidence for the coexistence of two magnetic phases in the $CeMn_2Ge_{1.0}Si_{1.0}$ sample was obtained using high resolution synchrotron X-ray diffraction; Fig. 6(a) indicates two distinct (101) reflections from ~80 K to ~180 K with a single (101) reflection observed above ~180 K. These structural features are entirely consistent with the occurrence of mixed structures of the ferromagnetic Fmc and

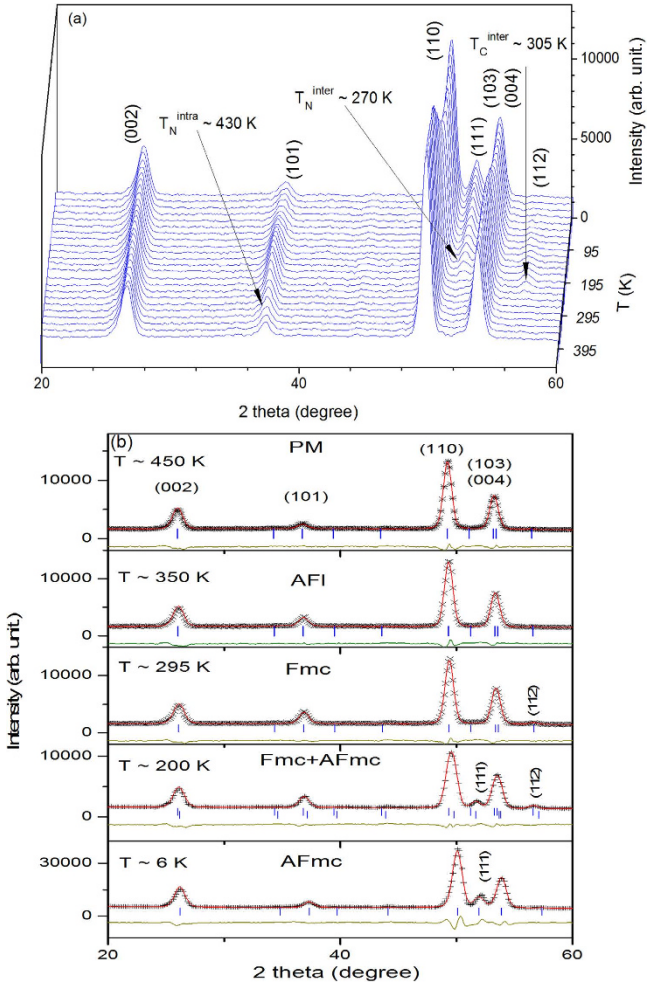

Figure 5. (**a**) Neutron diffraction patterns for $CeMn_2Ge_{0.8}Si_{1.2}$ over the temperature range 6–450 K and (**b**) Rietveld refinements for $CeMn_2Ge_{0.8}Si_{1.2}$ at 450 K, 350 K, 295 K, 200 K and 6 K ($\lambda = 2.4118$ Å , Wombat diffractometer, OPAL).

T (K)	6 K	200 K	200 K	295 K	350 K	450 K
Magnetic state	**AFmc**	**54% AFmc**	**46% Fmc**	**Fmc**	**AF/**	**PM**
a (Å)	4.0264(5)	4.0482	4.0831	4.0801	4.0846	4.0918
c (Å)	10.6335(4)	10.6479	10.7110	10.6889	10.7005	10.7235
z_{Ge}	0.3814	0.3818	0.3817	0.3814	0.3814	0.3814
μ_{ab} (μ_B)	0.76(8)	0.76	2.04	1.48	1.13	–
μ_c (μ_B)	2.00(6)	2.00	1.81	0.87	–	–
Canting angle	20.8	20.8	48.4	59.6	90	–
μ_{total} (μ_B)	2.14(9)	2.44	2.72	1.72	1.13	–
R_{wp}	9.52	7.18	7.18	6.14	6.67	6.52
R_{exp}	1.23	2.20	2.20	2.19	2.19	2.17

Table 2. Structural and magnetic parameters derived from Rietveld refinements of the neutron diffraction patterns for $CeMn_2Ge_{0.8}Si_{1.2}$. The errors are shown for the 6 K data as an example.

antiferromagnetic AFmc states below ~180 K. This behaviour was confirmed by comparison of the (101) peak for various $CeMn_2Ge_{2-x}Si_x$ compounds at 80 K (Fig. 6(b)). Comparison of these high resolution X-ray diffraction patterns reveals that only the $CeMn_2Ge_{1.0}Si_{1.0}$ sample exhibits mixed (101)-type peaks

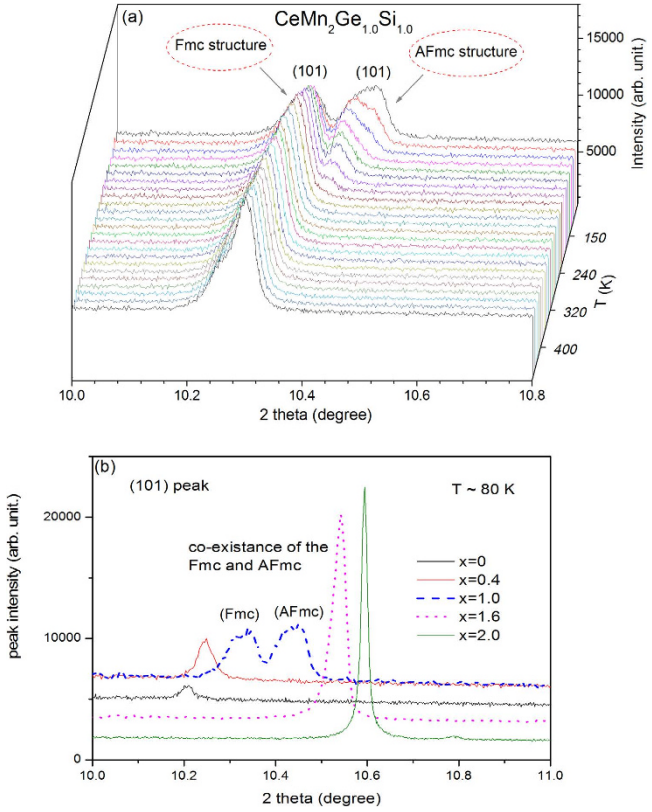

Figure 6. (**a**) X-ray diffraction patterns over the range of 80–450 K for $CeMn_2Ge_{1.0}Si_{1.0}$ in the 2Θ region around the (101) peak position, and (**b**) comparison of the reflections observed around the (101) peak position for $CeMn_2Ge_{2-x}Si_x$ compounds of Si concentrations x = 0.0, x = 0.4, x = 1.0, x = 1.6 and x = 2.0 at 80 K (λ = 0.6887 Å, Powder Diffract, Australian Synchrotron).

at 80 K compared with the single peak behaviour exhibited by $CeMn_2Ge_{2-x}Si_x$ compounds of Si concentrations x = 0.0, x = 0.4, x = 1.6 and x = 2.0. In addition co-existence of the (111) and (112) peaks as observed in the neutron diffraction patterns of $CeMn_2Ge_{0.8}Si_{1.2}$ below $T_N^{inter} \sim 270$ K (Fig. 5 at T ~ 200 K), indicates co-existence of two magnetic states corresponding to the ferromagnetic Fmc and antiferromagnetic AFmc states. This behaviour is similar to the co-existence of magnetic phases first reported in $La_{0.8}Y_{0.2}Mn_2Si_2$[34]. The Rietveld refinements also confirm that the unit cell for the AFmc phase is smaller than the unit cell for the Fmc phase (e.g. for $CeMn_2Ge_{0.8}Si_{1.2}$ at T = 200 K the unit cell volume V ~ 178.6 Å^3 for Fmc while V ~ 174.5 Å^3 for AFmc as listed in Table 2). This behaviour agrees well with the other re-entrant ferromagnetism systems[20,25,35], with around 0.3% contraction of the unit cell observed when the magnetic state changes at T_N^{inter} from Fmc to AFmc in $SmMn_2Ge_2$[35].

It is recognised that chemical distribution is expected on the mixed lattice site[3,7,29] in pseudo-ternaries. Although we can rule out long-range ordering of Si and Ge which would have been obvious due to substantial contrast in their neutron scattering lengths (4.15 fm and 8.19 fm, respectively), it is difficult to establish from neutron diffraction studies whether the distribution is completely random or some short-range ordering is present. Similar to our findings for the $PrMn_2Ge_{2-x}Si_x$ system[29], our high resolution synchrotron data of a series of $CeMn_2Ge_{2-x}Si_x$ samples (x = 0, 1.0, 1.6 and 2.0), at 450 K in the paramagnetic state (shown in Supplementary Figure S6) shows that the limiting compounds - $CeMn_2Si_2$ (of full width at half maximum for the (101) reflection of FWHM = 0.0103°) and $CeMn_2Ge_2$ (FWHM = 0.0305° for the (101) reflection), - have peak widths which are narrower than for samples with mixed Si and Ge (*e.g.* FWHM = 0.0361° and FWHM = 0.0587° for the (101) reflection of $CeMn_2Ge_{0.4}Si_{1.6}$ and $CeMn_2Ge_1Si_1$ respectively). These experimental findings demonstrate the occurrence of local stoichiometry fluctuations, particularly for the x = 1.0 sample. Rietveld analyses of high resolution synchrotron data for the $CeMn_2Ge_1Si_1$ sample in the paramagnetic state at 450 K, shows the presence of two phases with different concentrations: one is Si rich (53.5% phase fraction with a = 4.1006(8) Å and c = 10.7483(9) Å) and another is Ge rich (46.5% phase fraction with 4.1160(8) Å and c = 10.8091(9) Å). While the presence of these two phases due to stoichiometry fluctuations results in a width of the (101) peak at 450 K of around ~0.1°, the separation of the two (101) peaks is significantly larger (~0.26°; see 80 K synchrotron data of Fig. 6(b)) due to the presence of the two magnetic phases AFmc and Fmc. The average lattice strain ($\delta a/a$) values determined from Rietveld refinements of the high resolution synchrotron data of the $CeMn_2Ge_{2-x}Si_x$ compounds at 450 K in the paramagnetic state are: 0.012, 0.016, 0.019, 0.014 and 0.005

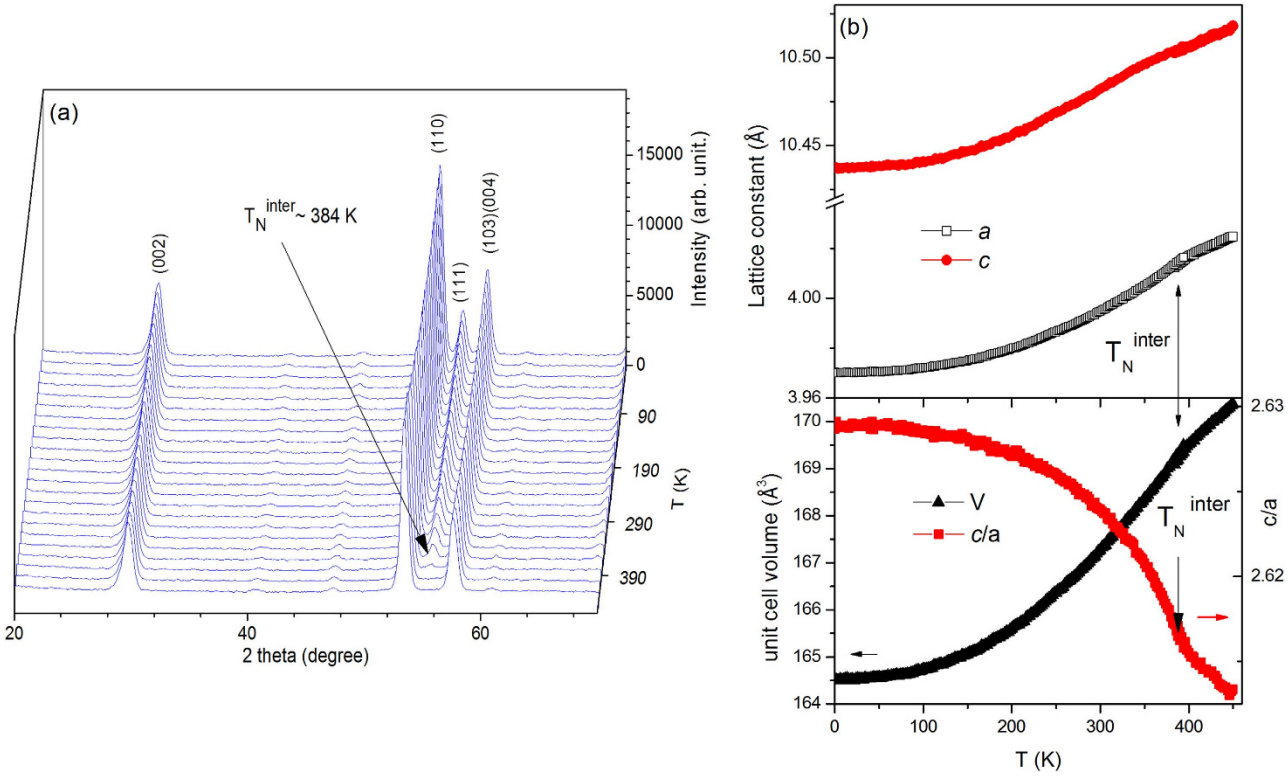

Figure 7. (**a**) Neutron diffraction patterns for $CeMn_2Si_2$ over the range of 6–450 K ($\lambda = 2.4118$ Å) and (**b**) Temperature dependences of the magnetic moment of $CeMn_2Si_2$ and the (111) peak (inset). (**c**) Temperature dependences of the lattice parameters *a* and *c* together with the unit cell volume, V, and axial ratio *c*/*a* for $CeMn_2Si_2$ as determined from Rietveld refinements of the neutron diffraction patterns.

for x = 0, 0.4, 1.0, 1.6 and 2.0 respectively (as shown in Figure S6). The variation in strain values with composition for $CeMn_2Ge_{2-x}Si_x$ displays similar trends to those observed in the $PrMn_2Ge_{2-x}Si_x$ system[29].

Details about the phase transitions in $CeMn_2Si_2$ over the temperature range 6–450 K were determined from neutron diffraction patterns obtained at temperature step intervals of 2 K (Fig. 7(a)). Rietveld refinements of the neutron diffraction pattern at 450 K confirm that $CeMn_2Si_2$ has the $ThCr_2Si_2$ structure as expected. The absence of magnetic scattering above $T_N^{intra} \sim 384$ K in reflections such as (101), (111) and (112) is consistent with a paramagnetic (PM) state (see e.g. the disordered magnetic states (PM) observed in $EuMn_2Si_2$[36] and $LaPrMn_2Si_2$[37]. Below $T_N^{intra} \sim 84$ K, $CeMn_2Si_2$ is found to exhibit the antiferromagnetic interlayer coupling structure (AFil) down to the experimental base temperature of T ~ 4 K (Fig. 7(c) and Table 1) in agreement with the findings of previous studies[18]. The AFil structure — a collinear antiferromagnetic structure between adjacent Mn planes in a + − + − sequence along the *c*-axis as depicted in Figure S1 — is indicated by the magnetic scattering observed at the (111), (113) and (201) reflections (extinction rules $h + k = 2n$ and $h + k + l = 2n + 1$) in agreement with those reported by Dincer *et al.*[37]. Figure 7(b) shows the temperature dependences (4–450 K) of the lattice parameters and *c*/*a* axial ratio as determined from Rietveld refinements of the neutron diffraction patterns. Both the *a* and *c* values exhibit a monotonic decrease with temperature in the region of the paramagnetic to interlayer antiferromagnetic transition. Furthermore, Fig. 7(b) reveals a significant change in the temperature dependence of the *c*/*a* ratio around $T_N^{inter} \sim 384$ K; this behaviour indicates strong coupling between the magnetism and the crystal lattice in the presence of a *c*-axis component of the Mn moment. As discussed recently[38], strong magnetostructural coupling leads to a large structural entropy change around the magnetic phase transition, thereby contributing to the total entropy change around the magnetic phase transition.

Magnetocaloric effect and critical exponent analysis. The magnetic entropy change, $-\Delta S_M$, has been determined for the set of $CeMn_2Ge_{2-x}Si_x$ compounds (x = 0.0–2.0) from their magnetization curves as functions of temperature and magnetic field (ΔB = 0–5 T) in the region around the ferromagnetic transition T_C^{inter}. The set of $-\Delta S_M$ values was determined by applying the standard Maxwell relation[39]:

$$-\Delta S_M(T, H) = \int_0^H \left(\frac{\partial M}{\partial T}\right)_H dH. \quad (2)$$

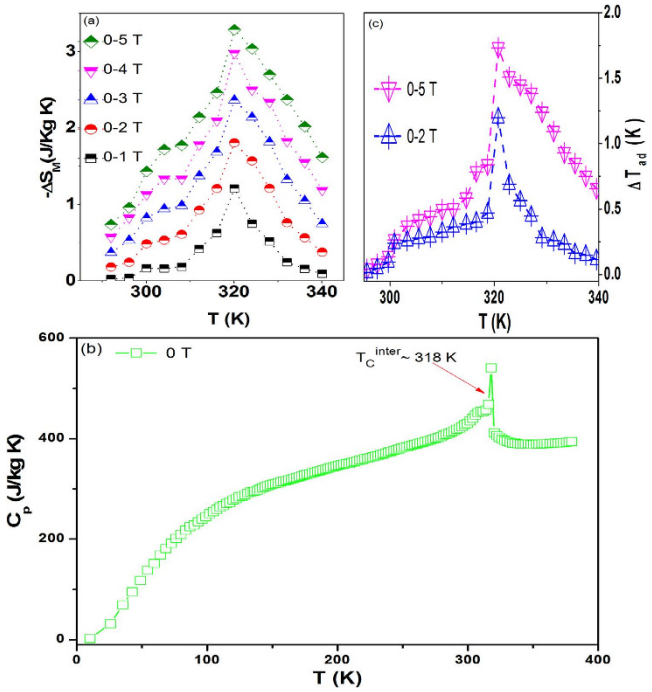

Figure 8. (**a**) Temperature dependence of the isothermal magnetic entropy change $-\Delta S_M$ for $CeMn_2Ge_2$ in the region around the ferromagnetic transition T_C^{inter} as determined from magnetisation measurements. (**b**) The heat capacity of $CeMn_2Ge_2$ as measured over the temperature range 10–340 K with no magnetic fields $B = 0$ T; (**c**) The adiabatic temperature change, ΔT_{ad}^{max}, for the $CeMn_2Ge_2$ compound.

As shown by the curves of Fig. 8(a), the $-\Delta S_M$ peak gradually broadens towards higher temperatures with increasing magnetic field (from $\Delta B = 0$–5 T), behaviour characteristic of a second order magnetic transition. The changes in magnetic entropy for the set of $CeMn_2Ge_{2-x}Si_x$ compounds (x = 0, 0.4 and 0.8) have been derived to be 3.21 J kg^{-1} K^{-1}, 2.86 J kg^{-1} K^{-1} and 2.67 J kg^{-1} K^{-1}, respectively (field change $\Delta B = 0$–5 T) around T_C^{Inter}. $CeMn_2Ge_{2-x}Si_x$ compounds exhibit moderate isothermal magnetic entropy accompanied with a second-order phase transition around room temperature comparable with other rare earth intermetallic compound in the RMn_2X_2 series. For example, Dincer and Elerman[40] obtained maximum entropy values in the approximate range $-\Delta S_M \sim 2$–3 J kg^{-1} K^{-1} ($\Delta B = 0$–5 T) around the Curie temperatures $T_C^{inter} \sim 300$–320 K for re-entrant $SmMn_{2-x}Fe_xGe2$ (x = 0.05, 0.10) and $SmMn_{2-x}Co_xGe_2$ (x = 0.05, 0.15) compounds. The present set of entropy values are also similar to other compound such as $Ho_2Fe_{15}Mn_2$ [41] ($-\Delta S_M = 2.7$ J kg^{-1} K^{-1} at 302 K) and Er_2Fe_{17} [42] ($-\Delta S_M = 3.6$ J kg^{-1} K^{-1} at 300 K).

The magnetic entropy change, $-\Delta S_M$ (T, B) has also been derived from heat calorimetric measurements of the field dependence of the heat capacity using the expression[43–45]:

$$-\Delta S_M(T, B) = \int_0^T \left(\frac{C(T, B) - C(T, 0)}{T} \right) dT \tag{3}$$

where $C(T,B)$ and $C(T,0)$ are the values of the heat capacity measured in field B and zero field, respectively. The corresponding adiabatic temperature change, ΔT_{ad} can be evaluated from $-\Delta S_M$ (T, B) and the zero field heat capacity data as:

$$\Delta T_{ad}(T, B) = \int_0^B \frac{T}{C_{B,P}} \left(\frac{\partial M}{\partial T} \right)_B dB. \tag{4}$$

Figure 8(b) show the set of heat capacity measurement obtained for $CeMn_2Ge_2$ with B = 0 T. The related peak in specific heat around $T_C^{inter} \sim 318$ K was found to decrease with increasing magnetic field. The ΔT_{ad} values derived from the specific heat data using equation (4) are shown in Fig. 8(c). The peak value of the adiabatic temperature change is found to be $\Delta T_{ad}^{max} = 1.7$ K for $\Delta B = 0$–5 T. Within experimental errors[23,46,47], the maximum magnetic entropy change for $CeMn_2Ge_2$ as determined from the heat capacity measurements of $-\Delta S_M^{max} \sim 2.9$ J kg^{-1} K^{-1} agrees well with the maximum entropy change $-\Delta S_M^{max} \sim 3.2$ J kg^{-1} K^{-1} determined from the magnetic measurements using the Maxwell relation.

Critical exponent analysis: Mean-field theory predicts that in the vicinity of second-order phase transitions, $-\Delta S_M$ is proportional to $(\mu_0 H/T_C)^{2/3}$ [Refs. 48, 49]. Figure 9(a) shows a graph of $-\Delta S_M$ as a

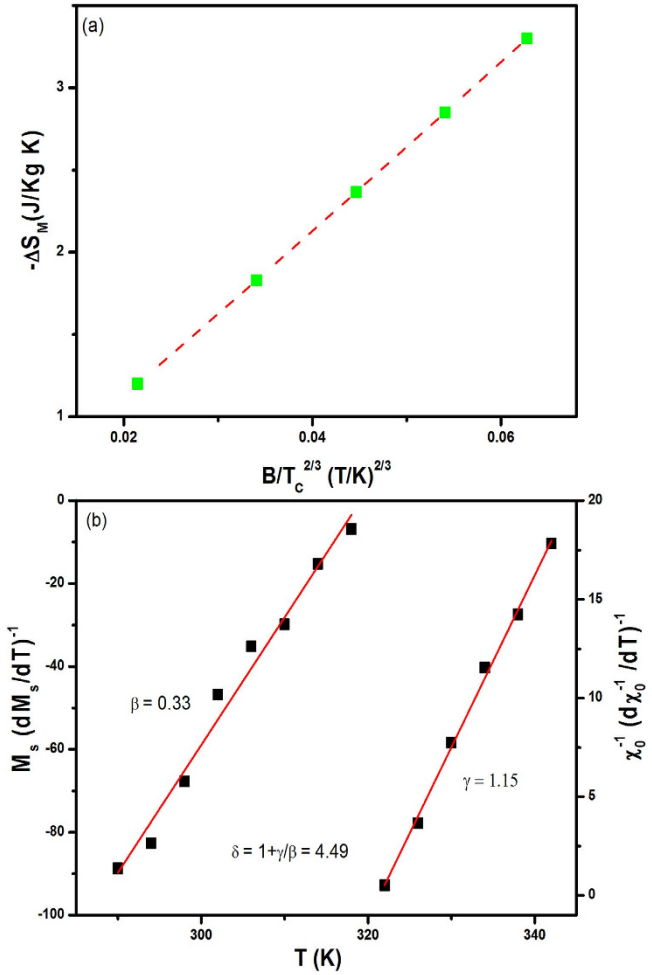

Figure 9. (**a**) Dependence of $-\Delta S_M$ (peak value of the magnetic entropy change at different B values) on the parameter $(B/T_C)^{2/3}$ for $CeMn_2Ge_2$ compound and (**b**) Kouvel–Fisher plots of $M_S(T)[dM_S/dT]^{-1}$ (left scale) and $\chi_0^{-1}(T)[d\chi_0^{-1}/dT]^{-1}$ (right scale) versus temperature. The lines are fits to the data around T_C as discussed in the text with fits leading to the critical exponent values.

function of $(B/T_C)^{2/3}$ in the region around the magnetic transition at $T_C^{inter} \sim 318$ K. The linear fit to the data in Fig. 9(a) clearly demonstrates that the relationship $-\Delta S_M \propto (B/T_C)^{2/3}$ is valid around the transition at T_C^{inter} for $CeMn_2Ge_2$. According to the conventional static scaling law, the critical properties of a second-order magnetic transition can be described by critical exponents β, γ and δ derived from magnetization measurements around the transition temperature. On applying these standard approaches, as shown by the fits to the Kouvel–Fisher plots of $M_S(T)[dM_S/dT]^{-1}$ and $\chi_0^{-1}(T)[d\chi_0^{-1}/dT]^{-1}$ versus temperature in Fig. 9(b), the critical exponents around T_C in $CeMn_2Ge_2$ have been determined to be $\beta = 0.33 \pm 0.03$ and $\gamma = 1.15 \pm 0.22$. Hence, on applying the relationship $\delta = 1 + \gamma/\beta$, with $\beta = 0.33$, $\gamma = 1.15$, the critical exponent $\delta = 1 + \gamma/\beta = 4.49 \pm 0.25$. The critical exponents derived from the analyses are similar to the theoretical values - $\beta = 0.365$, $\gamma = 1.386$ and $\delta = 4.80$ - based on the three-dimensional Heisenberg model corresponding to short range interactions[50]. Thus, the critical behaviour analysis in the vicinity of T_C^{inter} indicates that the magnetism of the $CeMn_2Ge_2$ compound is governed by short range interactions.

Discussion

The total magnetic moment of $CeMn_2Ge_{2-x}Si_x$ compounds at base temperature ~5 K is found to decrease with increasing Si content (see Table 1). This behaviour indicates that contraction of the unit cell leads to a reduction in the Mn moment value (e.g. $\mu_{Total} \sim 3.16\,\mu_B$ for $x = 0.0$ and $\mu_{Total} \sim 2.02\,\mu_B$ for $x = 2.0$) and agrees well with the tendency detected for both the $LaMn_2Ge_2$ and $LaMn_2Si_2$ systems where μ_{Total} is found to decrease with decrease in the lattice parameter a[51]. First principles calculations on $LaMn_2Si_2$ and $LaMn_2Ge_2$[51] suggest that the reduction of Mn moments in $LaMn_2Si_2$ ($a = 4.11$ Å) compared with $LaMn_2Ge_2$ ($a = 4.19$ Å) depends primarily on the Mn–Mn distances (stronger Mn–Mn hybridization due to shorter Mn–Mn distance leads to a smaller local Mn moment[19]). However the larger hybridization

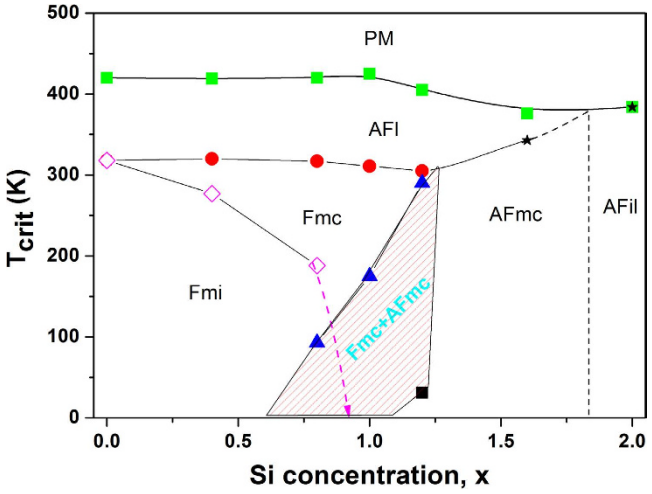

Figure 10. Magnetic phase diagram of $CeMn_2Ge_{2-x}Si_x$ as a function of Si content. As discussed in the text, T_N^{intra} (green squares) defines the transition from paramagnetism to intralayer antiferromagnetic ordering within the (001) Mn layers (AFl) (except x = 2.0 which exhibits AFil type antiferromagnetic order); T_C^{inter} (red circles) defines the transition from AFl to a canted spin structure (Fmc); Tc/c (open pink diamond) defines the transformation temperature of the magnetic structure from Fmc to a conical configuration Fmi type, T_N^{inter} (blue triangle) denotes the transition to the mixed region with co-existence of the antiferromagnetic canted structure AFmc and the Fmc structure. The dashed lines indicate trends in the data. As discussed in the text, the vertical dashed line located around Si concentration of x = 1.85 is used as a tentative guide to the boundary between the AFmc and AFil regions.

strength of Si–Mn in $LaMn_2Si_2$ than Ge–Mn in $LaMn_2Ge_2$ also plays a role. In the present study, the reduction of Mn moments in the $CeMn_2Ge_{2-x}Si_x$ compounds with increasing Si content can be ascribed to these two factors: (1) decrease of the Mn–Mn spacing (at room temperature ~300 K, $d_{Mn\text{-}Mn} = 2.93$ Å at $CeMn_2Ge_2$ to $d_{Mn\text{-}Mn} = 2.83$ Å at $CeMn_2Si_2$) and (2) increase of Si–Mn hybridization strengths compared with Ge–Mn hybridization[24], similar behaviour to that of $PrMn_2Ge_{2-x}Si_x$[25].

The temperature dependence of the $CeMn_2Ge_{2-x}Si_x$ lattice parameters demonstrates an anomaly in thermal expansion from low temperature to high temperature as indicated by the *c*/*a* ratio (for example $CeMn_2Ge_2$ in Fig. 4(c) and $CeMn_2Si_2$ in Fig. 7(b)) and is accompanied with the appearance of interlayer Mn–Mn interactions. This behaviour agrees well with others system as $PrMn_{2-x}Fe_xGe_x$ and $PrMn_2Ge_{2-x}Si_x$ where it is found that the interlayer Mn–Mn interactions rather than the intralayer Mn–Mn interactions, play the major role in the anomalous thermal expansion[30].

The present investigation of the magnetic and structural properties of a series of $CeMn_2Ge_{2-x}Si_x$ compounds (x = 0.0, 0.4, 0.8, 1.0, 1.2, 1.6 and x = 2.0) have enabled us to construct the magnetic phase diagram for the $CeMn_2Ge_{2-x}Si_x$ system as shown in Fig. 10 with more detail now available compared with previous studies[16]. The shaded region in Fig. 10 indicates the region of co-existence of the Fmc and AFmc phases as established here. The co-existence of different magnetic states at the same temperature is considered to be related to the non-random variation of site concentrations of Si and Ge, and depends sensitively on the Mn–Mn distances in this system; this in turn leads to differences in the local environments throughout the sample[7].

As expected, the magnetic states at room temperature have been modified by Si substitution due to the contraction of the unit cell indicated in Fig. 1. Samples with $x \geq 1.4$ where the lattice constant *a* is below $a_{crit1} \sim 4.06$ Å are antiferromagnetic at room temperature with no ferromagnetic order evident over the entire temperature range, whereas samples of Si content $x \leq 0.4$ are ferromagnetic at room temperature. It is interesting to note that samples with Si concentrations in the range x ~ 1.0–1.2 correspond approximately to the region of co-existence of the AFmc and Fmc phases around room temperature as shown in Fig. 10. A smaller unit cell in an antiferromagnetic state than in a ferromagnetic state (as indicated by the deviation from linear behaviour in the composition dependence of the lattice constants at room temperature; Fig. 1), can be understood in terms of the difference in magnetic states at room temperature for these samples and in turn reflects the large contribution from magnetic effects to thermal expansion[30].

The Si-rich compounds with $x \geq 1.85$ have a relatively simple magnetic behaviour, transforming from paramagnetism at high temperature to AFil. By comparison, Ge-rich samples (x ~ 0.0) successively exhibit two magnetic states as AFl and Fmi when cooling from the high temperature paramagnetic phase. As depicted in Fig. 10 , the Fmi structure was eliminated for Si concentrations $x \geq 1.0$, and co-existence of the AFmc and Fmc states is detected for $CeMn_2Ge_{2-x}Si_x$ in the intermediate Si concentration range $0.6 < x < 1.25$. Moreover, critical properties study on the second-order ferromagnetic transition of

$CeMn_2Ge_2$ demonstrate that the magnetic interactions around T_C^{inter} can be described with the three dimensional Heisenberg model corresponding to short range interactions. Overall this investigation has demonstrated that, as expected, the Si concentration plays the dominant role in tuning the magnetic structure and properties of the $CeMn_2Ge_{2-x}Si_x$ compounds.

Methods

$CeMn_2Ge_{2-x}Si_x$ alloys with Si concentrations $x = 0.0$, 0.4, 0.8, 1.0, 1.2, 1.6 and $x = 2.0$ were prepared by using standard arc melting with high purity elements on a water-cooled Cu hearth under purified argon gas. The mass loss of Mn during melting was compensated for by adding 3% excess Mn. The ingots were melted five times to attain homogeneity and then annealed at 900 °C for one week in an evacuated quartz tube. The samples were characterized by high intensity X-ray powder diffraction ($\lambda = 0.6887$ Å; 80–450 K) carried out at the Australian Synchrotron. The magnetic properties were investigated over the temperature range 6–350 K using the vibrating sample magnetometer option of a Quantum Design 14 T physical properties measurement system (PPMS). All samples were investigated by differential scanning calorimetry (DSC) to check for possible phase transitions in the higher temperature range from 300 K to 450 K. Specific heat measurements were carried out from 10 K to 360 K with applied field 0 T, 1 T, 2 T and 5 T. Neutron diffraction patterns were collected over the temperature range 6–450 K to cover the temperature range over which magnetic transitions were observed. The neutron diffraction experiments were carried out on the Wombat diffractometer (high intensity diffractometer; with $\lambda \sim 2.41$ Å), OPAL, Australia.

References

1. Siek, S., Szytuła, A. & Leciejewicz, J. Crystals and magnetic structure of RMn2Si2 (R = Pr, Nd, Y) and YMn2Ge2. *Solid State Communications* **39,** 863–866, doi:http://dx.doi.org/10.1016/0038-1098(81)90532-9 (1981).
2. Emre, B., Dincer, I., Elerman, Y. & Aksoy, S. An investigation of magnetocaloric effect and its implementation in critical behavior study of La1−xNdxMn2Si2 compounds. *Solid State Sciences* **22,** 1–7, doi:http://dx.doi.org/10.1016/j.solidstatesciences.2013.05.002 (2013).
3. Wang, J. L. *et al.* Driving Magnetostructural Transitions in Layered Intermetallic Compounds. *Physical Review Letters* **110,** 217211 (2013).
4. Wang, J. L., Campbell, S. J., Md Din, M. F., Kennedy, S. J. & Hofmann, M. Magnetic transitions and the magnetocaloric effect in the Pr1−xYxMn2Ge2 system. *physica status solidi (a)* **211,** 1092–1100, doi:10.1002/pssa.201330640 (2014).
5. Dincer, I. *et al.* Magnetic phase transitions in PrMn2−xCrxGe2. *Journal of Magnetism and Magnetic Materials* **248,** 268–275, doi:10.1016/s0304-8853(02)00349-9 (2002).
6. Dincer, I. *et al.* Neutron diffraction study of the magnetic structures of PrMn2−xCoxGe2 (x = 0.4, 0.5 and 0.8) with a new refinement procedure. *Journal of Physics: Condensed Matter* **16,** 2081 (2004).
7. Wang, J. L., Kennedy, S. J., Campbell, S. J., Hofmann, M. & Dou, S. X. Phase gap in pseudoternary R1−yRyMn2×2−xXx compounds. *Phys. Rev. B* **87,** 104401, doi:10.1103/PhysRevB.87.104401 (2013).
8. Welter, R., Venturini, G., Fruchart, D. & Malaman, B. Magnetic structures of PrMn2Si2 and NdMn2Si2 from neutron diffraction studies. *Journal of Alloys and Compounds* **191,** 263–270, doi:10.1016/0925-8388(93)90075-x (1993).
9. J. L. Wang *et al.* Magnetic phase transitions in Pr1−xLuxMn2Ge2 compounds *Journal of Physics: Condensed Matter* **21,** 124217 (2009).
10. Brabers, J. H. V. J., Buschow, K. H. J. & de Boer, F. R. Field-induced first-order antiferromagnetic-ferromagnetic transitions in RMn2Ge2 compounds and their relation to the magnetostriction of the Mn sublattice. *Physical Review B* **59,** 9314–9323 (1999).
11. Welter, R. & Malaman, B. Magnetic behaviour of the Mn sublattice in ThCr2Si2-type CaMn2−xFexGe2 solid solution investigated by magnetic measurements and neutron diffraction. *Journal of Alloys and Compounds* **354,** 35–46, doi:http://dx.doi.org/10.1016/S0925-8388(02)01354-3 (2003).
12. Din, M. F. M. *et al.* Magnetic properties and magnetocaloric effect of NdMn2− xTixSi2 compounds. *Journal of Physics D: Applied Physics* **46,** 445002 (2013).
13. Hofmann, M., Campbell, S. J., Knorr, K., Hull, S. & Ksenofontov, V. Pressure-induced magnetic transitions in $LaMn_2Si_2$. *Journal of Applied Physics* **91,** 8126–8128, doi:doi:http://dx.doi.org/10.1063/1.1456433 (2002).
14. Kumar, P. *et al.* Pressure-induced changes in the magnetic and magnetocaloric properties of RMn2Ge2 (R = Sm,Gd). *Physical Review B* **77,** 224427 (2008).
15. Md Din, M. F. *et al.* Magnetic phase transitions and entropy change in layered NdMn1.7Cr0.3Si2. *Applied Physics Letters* **104,** 042401, doi:http://dx.doi.org/10.1063/1.4863230 (2014).
16. Liang, G. & Croft, M. Ce-valence instability in the antiferromagnetic and ferromagnetic host series CeMn2(Si1-xGex)2. *Phys. Rev. B* **40,** 361, doi:10.1103/PhysRevB.40.361 (1989).
17. Venturini, G., Malaman, B. & Ressouche, E. Magnetic ordering in ternary RMn2Ge2 compounds (R =Tb, Ho, Er, Tm, Lu) from neutron diffraction study. *Journal of Alloys and Compounds* **240,** 139–150, doi:http://dx.doi.org/10.1016/0925-8388(96)02272-4 (1996).
18. Fernandez-Baca, J. A., Hill, P., Chakoumakos, B. C. & Ali, N. Neutron diffraction study of the magnetic structures of CeMn2Ge2 and CeMn2Si2. *Journal of Applied Physics* **79,** 5398–5400, doi:http://dx.doi.org/10.1063/1.362317 (1996).
19. Welter, R., Venturini, G., Ressouche, E. & Malaman, B. Neutron diffraction study of CeMn2Ge2, PrMn2Ge2 and NdMn2Ge2: evidence of dominant antiferromagnetic components within the (001) Mn planes in ferromagnetic ThCr2Si2-type manganese ternary compounds. *Journal of Alloys and Compounds* **218,** 204–215, doi:http://dx.doi.org/10.1016/0925-8388(94)01378-0 (1995).
20. Venturini, G., Malaman, B. & Ressouche, E. Investigations of the solid solution NdMn2−xFexGe2 (x = 0.1−1.4) by magnetic measurements and neutron diffraction. *Journal of Alloys and Compounds* **237,** 61–73, doi:http://dx.doi.org/10.1016/0925-8388(95)02177-9 (1996).
21. Pecharsky, V. K. & Gschneidner Jr, K. A. Effect of alloying on the giant magnetocaloric effect of Gd5(Si2Ge2). *Journal of Magnetism and Magnetic Materials* **167,** L179–L184 (1997).
22. K. A. Gschneidner Jr, V. K. Pecharsky & Tsokol, A. O. *Rep. Prog. Phys.* **68** (2005).
23. Pecharsky, V. K. & Gschneidner, J. K. A. Giant Magnetocaloric Effect in Gd5(Si2Ge2). *Physical Review Letters* **78,** 4494–4497 (1997).
24. L. B. McCusker, R. B. Von Dreele, D. E. Cox, D. Louër & Scardi, P. Rietveld refinement guidelines. *Journal of Applied Crystallography* **32,** 36–50, doi:10.1107/S0021889898009856 (1999).

25. Wang, J. L. *et al.* Magnetism and magnetic structures of PrMn2Ge2−xSix. *Journal of Physics: Condensed Matter* **25,** 386003 (2013).
26. Kennedy, S., Wang, J., Campbell, S., Hofmann, M. & Dou, S. Pressure induced magneto-structural phase transitions in layered RMn2X2 compounds (invited). *Journal of Applied Physics* **115,** 172617, doi:http://dx.doi.org/10.1063/1.4870582 (2014).
27. Gelato, L. BLOKJE, a computer program to calculate the domain of an atom in a structure. *J. Appl. Crystallogr.* **14,** 151 (1981).
28. Fukuhara, T., Maezawa, K., Ohkuni, H., Kagayama, T. & Oomi, G. High-pressure resistivity and lattice parameters of CeNi2Ge2. *Physica B: Condensed Matter* **230–232**, 198–200, doi:10.1016/s0921-4526(96)00589-3 (1997).
29. Di Napoli, S., Llois, A. M., Bihlmayer, G. & Blügel, S. Magnetic order in RMn2Ge2 (R = Y,Ca) compounds and their solid solutions with $LaMn_2Ge_2$. *Physical Review B* **75,** 104406 (2007).
30. Wang, J. L. *et al.* Magnetic structures and phase transitions in PrMn2−xFexGe2. *Journal of Applied Physics* **104,** doi:http://dx.doi.org/10.1063/1.3021096 (2008).
31. Venturini, G., Welter, R., Ressouche, E. & Malaman, B. Neutron diffraction studies of $LaMn_2Ge_2$ and $LaMn_2Si_2$ compounds: evidence of dominant antiferromagnetic components within the Mn planes. *Journal of Alloys and Compounds* **210,** 213–220, doi:http://dx.doi.org/10.1016/0925-8388(94)90141-4 (1994).
32. Wang, J. L. *et al.* Magnetic structures and phase transitions in PrMn2-xFexGe2. *Journal of Applied Physics* **104,** 103911–103912 (2008).
33. Wang, J. L. *et al.* Substitution of Y for Pr in PrMn2Ge2—The magnetism of Pr0.8Y0.2Mn2Ge2. *Journal of Applied Physics* **113,** doi:http://dx.doi.org/10.1063/1.4798622 (2013).
34. Hofmann, M., Campbell, S. J. & Kennedy, S. J. Competing magnetic interactions in La0.8Y0.2Mn2Si2 - coexistence of canted ferromagnetism and antiferromagnetism. *Journal of Physics: Condensed Matter* **12,** 3241 (2000).
35. Duraj, M., Duraj, R., Szytuła, A. & Tomkowicz, Z. Magnetic properties of SmMn2Ge2 compounds. *Journal of Magnetism and Magnetic Materials* **73,** 240–246, doi:http://dx.doi.org/10.1016/0304-8853(88)90300-9 (1988).
36. Hofmann, M., Campbell, S. J. & Edge, A. V. J. EuMn2Ge2 and EuMn2Si2: Magnetic structures and valence transitions. *Physical Review B* **69,** 174432 (2004).
37. Dincer, I., Elerman, Y., Elmali, A., Ehrenberg, H. & André, G. Neutron diffraction study of the La1-xPrxMn2Si2 (x=0.4, 0.7 and 1) compounds and the general description of the magnetic behavior of Mn in RMn2Ge2 and RMn2Si2. *Journal of Magnetism and Magnetic Materials* **313,** 342–353, doi:http://dx.doi.org/10.1016/j.jmmm.2006.12.032 (2007).
38. Gschneidner Jr, K. A., Mudryk, Y. & Pecharsky, V. K. On the nature of the magnetocaloric effect of the first-order magnetostructural transition. *Scripta Materialia* **67,** 572–577, doi:10.1016/j.scriptamat.2011.12.042 (2012).
39. Feng Xia, H., Bao Gen, S., Ji Rong, S., Zhao Hua, C. & Xi Xiang, Z. Magnetic entropy change in La(Fe0.98Co0.02)11.7Al13. *Journal of Physics: Condensed Matter* **12,** L691 (2000).
40. Dincer, I. & Elerman, Y. The influence of substitution of Mn by Fe and Co on magnetocaloric effect and magnetoresistance properties of SmMn2Ge2. *Journal of Magnetism and Magnetic Materials* **326,** 50–57, doi:http://dx.doi.org/10.1016/j.jmmm.2012.08.007 (2013).
41. Wang, J. L. *et al.* Magnetovolume effect in Ho2Fe17-xMnx compounds. *Journal of Applied Physics* **111,** doi:http://dx.doi.org/10.1063/1.3671422 (2012).
42. Zhang, X. X., Wang, F. W. & Wen, G. H. Magnetic entropy change in RCoAl (R = Gd, Tb, Dy, and Ho) compounds: candidate materials for providing magnetic refrigeration in the temperature range 10 K to 100 K. *Journal of Physics: Condensed Matter* **13,** L747 (2001).
43. Pecharsky, V. K. & Gschneidner, J. K. A. Magnetocaloric effect from indirect measurements: Magnetization and heat capacity. *Journal of Applied Physics* **86,** 565–575 (1999).
44. Ekkes, B. Developments in magnetocaloric refrigeration. *Journal of Physics D: Applied Physics* **38,** R381 (2005).
45. Gschneidner Jr, K. A. & Pecharsky, V. K. Thirty years of near room temperature magnetic cooling: Where we are today and future prospects. *International Journal of Refrigeration* **31,** 945–961, doi:10.1016/j.ijrefrig.2008.01.004 (2008).
46. Gschneidner Jr, K. A., Pecharsky, V. K. & Tsokol, A. O. Recent developments in magnetocaloric materials. *Reports on Progress in Physics* **68,** 1479 (2005).
47. Wang, J. L. *et al.* Magnetocaloric effect in layered $NdMn_2Ge_{0.4}Si_{1.6}$. *Applied Physics Letters* **98,** 232509–232503 (2011).
48. Oesterreicher, H. & Parker, F. T. Magnetic cooling near Curie temperatures above 300 K. *Journal of Applied Physics* **55,** 4334–4338, doi:http://dx.doi.org/10.1063/1.333046 (1984).
49. Wang, J. L. *et al.* Re-entrant ferromagnet PrMn2Ge0.8Si1.2: Magnetocaloric effect. *Journal of Applied Physics* **105,** doi:http://dx.doi.org/10.1063/1.3059610 (2009).
50. Kaul, S. N. Static critical phenomena in ferromagnets with quenched disorder. *Journal of Magnetism and Magnetic Materials* **53,** 5–53, doi:http://dx.doi.org/10.1016/0304-8853(85)90128-3 (1985).
51. Di Napoli, S. *et al.* Magnetic structure and transport properties of noncollinear LaMn2X2(X=Ge,Si) systems. *Phys. Rev. B* **70,** 174418, doi:10.1103/PhysRevB.70.174418 (2004).

Acknowledgments

We would like to thank Dr. Qinfen Gu from the Australian Synchrotron for assistance with the high resolution X-ray diffraction experiments. Moreover, we appreciate very much the help from Dr. Helen Maynard- Casely during our neutron diffration experiments at OPAL, ANSTO Australia. This research was supported by Australian Research Council Discovery Projects (DP0879070, DP110102386 and DP120100095).

Author Contributions

M.F.M.D. and J.L.W. designed this study. Z.X.C. and M.A. contributed to the data analyses. S.X.D., S.J.K. and S.J.C. provided suggestions for the analyses and the manuscript. All contributed in completing the manuscript and approved the final manuscript. All authors, particularly J.L.W, M.F.M.D. and S.J.C. reviewed the manuscript.

Additional Information

Supplementary information accompanies this paper at http://www.nature.com/srep

Competing financial interests: The authors declare no competing financial interests.

How to cite this article: Md Din, M. F. *et al.* Tuneable Magnetic Phase Transitions in Layered $CeMn_2Ge_{2-x}Si_x$ Compounds. *Sci. Rep.* **5**, 11288; doi: 10.1038/srep11288 (2015).